4.5 FLASH RATE, ELECTRICAL, MICROPHYSISCAL, AND DYNAMICAL RELATIONSHIPS ACROSS A SIMULATED STORM SPECTRUM

Ariel Cohen[1,*] and Edward Mansell[2]
[1]CIMMS/Univ. of Oklahoma and NOAA/OAR/NSSL, Norman, OK
NOAA/NWS Great Falls (+), MT
[2]NOAA/OAR/National Severe Storms Laboratory, Norman, OK, U.S.A.

1. Introduction

A common problem in convective forecasting is the prediction of lightning flash rates, particularly of cloud-to-ground (CG) flashes. Developing a solution to this problem is restricted by the spatially and temporally finite observing system of lightning and its potential predictors. Observational studies have analyzed CG flash onset (e.g., Hondl and Eilts 1994; Gremillion and Orville 1999) and storm-flash rate relationships (e.g., MacGorman et al. 1989; Carey and Rutledge 1996; Wiens et al. 2005; Petersen et al. 2005). Kuhlman et al. (2006) presented model-based flash rate relationships for the tornadic supercell storm studied by Wiens et al. (2005). Both studies found good correlations between total flash rate and both graupel echo volume and updraft volume. Petersen et al. (2005) found a high correlation between total flash rate and ice-water path (IWP, a measure of integrated graupel mass) over a large range of convection type, but typically with only about 80 s of data from any given storm (the viewing time of the satellite). The goal of the present study is to evaluate some of the predictors for flash rates from an ensemble of simulated non-severe convective storms to have both a range of storm type as in Petersen et al. (2005) and histories of individual cases. Thus it will be possible to compare the range of relationships of individual storms with aggregate behavior.

In this study, we use the results of twenty-two simulations run by COMMAS to develop the relationships between flash rates and several of its potential predictors.

2. Cloud Model

The numerical model used in this study is the Collaborative Model for Multiscale Atmospheric Simulation (COMMAS; Wicker and Wilhelmson 1995; Wicker and Skamarock 2002; Coniglio et al. 2006). COMMAS uses the basic equation set from Klemp and Wilhelmson (1978) and prognostic equations are included for momentum, pressure, potential temperature, and turbulent kinetic energy (Deardorff 1980). Time integration is performed with a third-order Runge–Kutta scheme (Wicker and Skamarock 2002). The basic microphysical model used for this study is a 3-ICE microphysics scheme (Ziegler 1985; Zrnić et al. 1993) that predicts mass and number concentration for five hydrometeor types (droplets, rain, ice crystals, snow, and graupel). The two-moment scheme also predicts the concentration of cloud condensation nuclei (CCN) and predicts the average graupel bulk density, which is allowed to vary between 300 to 900 kg m^{-3}. For this simulation, initial CCN concentration was set at $700(\rho_{\rm air}/\rho_o)$ cm^{-3}, where $\rho_{\rm air}$ is air density and $\rho_o = 1.0$ kg m^{-3}.

Electrification processes (Mansell et al. 2005) include parameterizations of multiple laboratory results of noninductive charge separation in rebounding graupel-ice collisions. Small ion processes such as attachment and drift motion are treated explicitly. The branched lightning parameterization of Mansell et al. (2002) was used, with charge neutrality of the channel structure now maintained by adjusting the electric potential of the channel (e.g., Mazur and Ruhnke 1998). In Mansell et al. (2002), a simple height threshold (typically 2 km) was used to declare a flash to be a CG (i.e., the flash was not required to propagate all the way to ground). In the updated scheme, the potential at the tip must maintain the correct sign to be connected to ground, since the sign can change due to internal resistance and adjustment of the channel potential.

Simulations were carried out on a model domain using dimensions 100x100x17 km^3 (200x200x45 grid points). The horizontal resolution was 500 m, and the vertical spacing stretched from 200 m in the lowest level of the model to

* *Corresponding author address*: Ariel Cohen, National Weather Service, Great Falls Weather Forecast Office, 5324 Tri-Hill Frontage Rd., Great Falls, MT 59404; *e-mail: Ariel.Cohen@noaa.gov.*

Case	w	Shr Mag	Shr Dpt
Ashtabula +	11.2	25.0	3500.
Butler +	12.5	25.0	3500.
Cuyahoga +	12.5	19.0	1000.
Delaware +	12.6	25.0	6000.
Fayette +	12.5	25.0	3500.
Franklin +	13.0	35.0	5555
Greene +	13.0	10.0	6666
Hardin +	10.0	40.0	7563
Harrison +	11.5	17.5	1193
Jefferson +	13.0	40.0	6688
Warren +	*	*	*
Ashtabula ++	11.2	25.0	3500.
Butler ++	12.5	25.0	3500.
Cuyahoga ++	12.5	19.0	1000.
Delaware ++	12.6	25.0	6000.
Fayette ++	12.5	25.0	3500.
Franklin ++	13.0	35.0	5555
Greene ++	13.0	10.0	6666
Hardin ++	10.0	40.0	7563
Harrison ++	11.5	17.5	1193
Jefferson ++	13.0	40.0	6688
Warren ++	*	*	*

Table 1: Environmental initialization for each storm (single asterisk denotes the environmental conditions associated with the 2 June 1995, Dimmit, TX, tornadic storm, with w denoting surface mixing ratio with units $g\ kg^{-1}$), Shr Mag denoting shear magnitude with units s^{-1}, Shr Dpt denoting shear depth with units m, with a single plus sign indicating an SP storm, and with a double plus sign indicating a TAK storm)

Case	Correlation Coefficient		
	EF	GV	UMF
Ashtabula +	0.40	0.89	0.89
Butler +	0.24	0.84	0.77
Cuyahoga + *	0.18	0.66	0.09
Delaware +	0.35	0.77	0.52
Fayette + *	0.17	0.74	negl.
Franklin +	0.19	0.80	0.79
Greene + *	0.13	0.81	0.01
Hardin +	0.29	0.53	0.57
Harrison + *	0.12	0.65	0.58
Jefferson +	0.25	0.82	0.70
Warren +	0.35	0.79	0.78
Ashtabula ++	0.24	0.88	0.86
Butler ++	0.28	0.80	0.78
Cuyahoga ++ *	0.18	0.68	0.05
Delaware ++	0.25	0.78	0.54
Fayette ++ *	0.08	0.72	negl.
Franklin ++	0.20	0.82	0.78
Greene ++ *	0.05	0.50	0.01
Hardin ++	0.54	0.63	0.58
Harrison ++ *	0.21	0.66	0.50
Jefferson ++	0.26	0.75	0.64
Warren ++	0.31	0.83	0.82

Table 2: Raw CCs between flash rate and electric field (EF), graupel volume (GV), and updraft mass flux (UMF), with no trend removal. An asterisk (*) denotes a simulation involving unicellular storm mode for the majority of the simulation. A (+) sign indicates an SP storm, and (++) sign indicates a TAK storm, with "negl." indicating a negligible value below 0.01

500 m at 10 km altitude and above. For all cases, convection was initiated by a region of vertical acceleration in the model domain, along with random thermal perturbations over the model domain. Grid motion was chosen to retain storms within the model domain. Each case was run for two hours. While a few storms dissipated before the end of this two-hour period, most storms were still actively producing lightning at the end of the two-hour period.

Eleven of the storms (indicated by a + sign, and also referred to as SP) use the Saunders and Peck (1998) charging regime to study their electrical properties. Another set of eleven storms (indicated by a ++ sign, and also referred to as TAK) assume the same environmental shear magnitude, shear depth, and surface mixing ratio to initialize each storm as the first set, however all of the second set used the Takahashi (1984) charging parameterization. The difference between the two charging schemes lies in the relationship between ambient temperature and cloud water content or graupel rime accretion rate (e.g., see Mansell et al. 2005). The appendix contains simulated reflectivity plan views at a specified time for each of the eleven unique storms.

Table 1 lists two sets of eleven cases, as well as the nomenclature used, for a total twenty-two cases. Since the only difference between the two sets of storms is the noninductive charging parameterization, the non-electrical properties of the two sets are identical. The environmental shear magnitude, shear depth, and surface mixing ratio used to initialize each storm varied from storm to storm. The vertical wind, temperature, and dewpoint profiles in each simulation are specified by Weisman and Klemp (1982) and Weisman and Klemp (1984), except for the Fayette (SP and TAK) and Warren (SP and TAK)

simulations. The Warren storm was initialized using the proximity sounding from the 2 June 1995 the Dimmitt, Texas tornado as described in Fierro et al. (2006), while the Fayette simulation was initialized using a hand-made sounding. The environmental conditions were assumed to be horizontally homogeneous across the domain initially.

3. Individual Storm Discussion

By generating time series of several different variables for each simulation, we are able to study the numerous relationships that exist between the variables. To understand the most basic dependencies in the most consistent way possible, we chose to study the strength of linear relationships. This provides a basic guide of the degree to which microphyiscal, dynamical, and electrical variables explain flash rates. The raw correlation coefficients (CC), without any shifting of the time series, between maximum electric field over the domain, graupel volume, and updraft mass flux across the 0°C isotherm are displayed in Table 2.

For most simulations, the relationship between flash rate and electric field is weak. Raw correlation coefficients between these two variables rarely exceed 0.4, with most correlation coefficients below 0.3. The electric field time series data (not shown) suggest that, in most cases, the electric field rapidly increases in the incipient stages of the storm, and peaks at a value generally between 80 kV m^{-1} and 100 kV m^{-1}, the nature of which is discussed by MacGorman and Rust (1998). This value can be considered a proxy for the electric field strength that promotes electrical breakdown, and the development of flashes. Once this value is achieved, however, flash rates can continue to increase but electric field strengths do not. This is consistent with the concept that flashes serve the purpose of limiting the electric field strength within storms, which is a fundamental assumption of the electrical structure of any numerical model, as discussed in Mansell et al. (2002) and Mansell et al. (2005).

Several microphysical and kinematic variables could potentially serve as predictors for flash rates. We will consider each one separately. Carey and Rutledge (1996) considered these relationships for a specific storm that occurred on 21 May 1993 on the Front Range of Colorado, which was sampled by the CSU-CHILL doppler radar. Their study drew many conclusions regarding predictors for intracloud flashes for that storm, including graupel volume. Some of the results of that study are compared to the present study.

As in Carey and Rutledge (1996), we find a very strong relationship between flash rate and graupel volume. In fact, the correlation coefficients between graupel volume and flash rate are always above 0.400, and often above 0.700, suggesting this strong relationship. The correlation between flash rate and updraft mass flux across the 0 °C isotherm is also significant. The physical relationship between updraft mass flux, convective-scale charge separation, and flash rate is consistent with this signal, as cited in Carey and Rutledge (1996). Additionally, graupel volume is causally related to updraft mass flux, so it is not surprising that both are correlated with flash rate. On average, however, the correlation coefficients between updraft mass flux and flash rate are smaller than between graupel volume and flash rate.

The relationship between graupel volume and flash rate and between updraft mass flux and flash rate are the strongest in the cases reminiscent of supercells (based on hook echo identification). This is the case for the Ashtabula (SP and TAK), Butler (SP and TAK), Delaware (SP and TAK), and Warren (SP and TAK) simulations, with correlation coefficients are generally over 0.200 larger than most other simulations.

Correlation coefficients were also calculated after linear trends were removed (Table 3). The correlation coefficients between the detrended electric field and detrended flash rate were negligible, suggesting no significant relationship between the cycles of these variables. The correlations between flash rate perturbations and graupel volume perturbations, however, were negligible or marginally significant for 7 cases (both SP and TAK), but significant (> 0.45) for the other 4 (Cuyahoga, Fayette, Greene, and Harrison). The cases for which the largest correlation coefficients exist between perturbation graupel volume and perturbation flash rate are ones in which the convection was largely unicellular for the entire 2-hr simulation. This suggests that low detrended correlations may have resulted from multiple cells in the domain at different stages of maturity or simply a storm mode that has greater short-term variability. Section 6 discusses results from extracting time-series for a subdomain of three low-correlation cases.

The correlations between CG flash rate and electric field, graupel volume, and updraft mass flux were not significant (< 0.3) especially between flash rate and electric field, graupel volume, and updraft mass flux (not shown). This poor relationship is likely due to the rarity and ran-

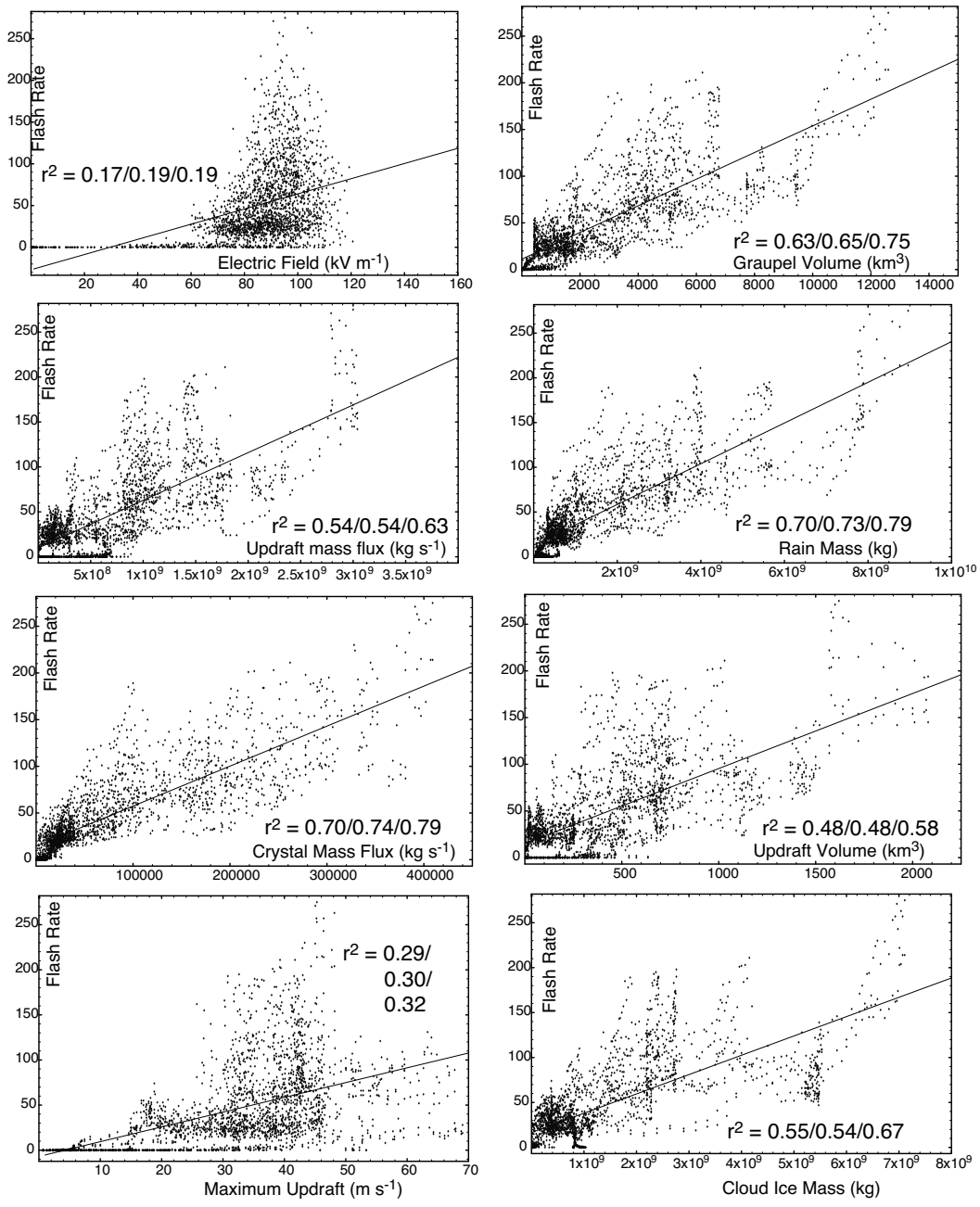

Figure 1: Summary scatterplots of flash rate and CG flash rate versus electric field, graupel volume, updraft mass flux, rain mass, crystal mass flux, updraft volume, maximum updraft, and cloud ice mass, with linear fits superimposed. Correlation coefficients are given for all cases and for SP and TAK separately (ALL/SP/TAK).

Case	Correlation Coefficient		
	EF	GV	UMF
Ashtabula +	0.01	negl.	negl.
Butler +	0.06	negl.	negl.
Cuyahoga + *	negl.	0.74	0.01
Delaware +	negl.	negl.	0.01
Fayette + *	0.25	0.68	0.08
Franklin +	0.01	0.38	0.14
Greene + *	0.26	0.76	0.10
Hardin +	negl.	0.05	0.23
Harrison + *	0.01	0.74	0.42
Jefferson +	0.01	0.03	0.19
Warren +	0.02	0.06	negl.
Ashtabula ++	negl.	0.41	0.14
Butler ++	0.01	0.04	negl.
Cuyahoga ++ *	negl.	0.66	negl.
Delaware ++	0.03	0.05	negl.
Fayette ++ *	0.25	0.62	0.07
Franklin ++	0.01	0.12	0.19
Greene ++ *	0.25	0.46	0.16
Hardin ++	0.04	negl.	0.25
Harrison ++ *	0.01	0.73	0.30
Jefferson ++	negl.	0.07	0.22
Warren ++	0.01	0.03	0.01

Table 3: CCs between flash rate and electric field (EF), graupel volume (GV), and updraft mass flux (UMF), with CCs between detrended value in parentheses, with an asterisk denoting a simulation involving unicellular storm mode for the majority of the simulation, with a single plus sign indicating an SP storm, with a double plus sign indicating a TAK storm, and with "negl." indicating a negligible value below 0.01

dom occurrence of CG flashes compared to intracloud flashes, which can be visualized by cross referencing the time series of flash rate versus CG flash rate for each simulation. Naturally, the correlation coefficients between the perturbation forms of these quantities are also negligibly small, indicating very weak relationships between the cycles of CG flashes and electric field, graupel volume, and updraft mass flux.

The graupel volume and updraft mass flux time series data were also subjected to Fourier cross-correlation to determine whether correlation values (especially for detrended variables) with flash rate could be increased by phase-shifting (e.g., MacGorman et al. 1989; Wiens et al. 2005). The lag time to maximize the correlation coefficients was generally zero or on the order of a few minutes. Any increase in the detrended correlations, however, was not significant.

4. Aggregated Storms Discussion

We will now consider relationships among several flash rate predictors in an aggregate sense. A potential disadvantage to this analysis is that combining time series from several different simulations implies a loss of detail for individual storm simulations. Nevertheless, this analysis provides an overall summary for the range of values and relationships discussed in this study. Figure 1 shows the relationships series for all the aforementioned variables, as well as for rain mass, crystal mass flux through the -30 °C isotherm, the updraft volume for updrafts in excess of 10 m s^{-1}, maximum updraft, and cloud ice mass.

Similar to the individual simulations, the relationship between aggregate flash rate and graupel volume is significant, with slightly higher correlations for rain mass and ice crystal mass flux. Petersen et al. (2005) also determined a strong statistical relationship between flash density and graupel mass from sampling a wide range of convection. Other studies, including Kempf and Krider (2003) have also showed a relationship between CG flash rates and surface rain rates, which in turn are conceivably highly correlated with melting graupel. Electric field similarly shows poor correlation, as well as maximum updraft speed, neither of which gives an integrated measure of storm vigor.

Graupel volume, updraft mass flux, and cloud ice mass are also well-correlated with flash rates in an aggregated sense. These three variables are directly related to the processes responsible for charge separation discussed earlier. The updraft mass flux is associated with the distribution of positively-charged cloud ice particles into the upper parts of the storm and negatively-charged graupel particles into the bottom part of the storm. On the other hand, the relationship between flash rate and updraft volume is relatively weaker, and yet even weaker for maximum updraft. This suggests that the particle phase relationships and distributions play a more significant role in the relationship between the updraft mass flux and the flash rate than then updraft strength itself.

The relationships between CG flash rates and all the variables discussed in this work (not shown) are all very weak, as the number of CG flashes is quite variable over a large range of the values of these quantities. Note that the CG flash rate is a small fraction of the total simulated flash rate, and it is possible that the model does not always simulate realistic CG flash rates (Mansell et al. 2002).

5. Charging Scheme Discussion

We can also compare the difference between the SP and TAK charging schemes. Since the microphysics package is independent of the charging scheme selected, the time series of graupel volume, updraft mass flux, rain mass, crystal mass flux, updraft volume, maximum updraft, and cloud ice mass are the same for the TAK storms as for the SP storms. Variations in flash rate and electric field time series between TAK and SP storms, however, result in variations in the flash rate relationships between each TAK and corresponding SP storm. While the same general relationships hold – positive ones – some differences do exist. On a storm-by-storm basis, the correlations are quite similar (Table 2), but when the cases are aggregated separately by charging scheme, the linear relationships are consistently stronger for the TAK charging scheme than for SP charging scheme by as much as 0.1.

The total amounts of positive and negative charge gained by graupel from noninductive charging was determined by integrating the charge separation rates over time and space across the entire model domain. Both the total positive and negative charge were computed for all 22 simulations, resulting in comparisons among SP and TAK storm pairs. Figure 2 displays a scatterplot of these totals, where each SP-TAK storm pair is connected with a thin line. The total negative charge for any simulation using the SP scheme is substantially more negative than using the TAK scheme, while the total positive charge for any simulation using the TAK is generally slightly smaller than using the SP scheme. In a couple pairs, the total positive charge is larger using the TAK instead of the SP scheme. Thus, the total amount of noninductive charge transfer is larger when using the SP scheme than when using the TAK scheme. And, the main contributor to the larger amount of charge transferred in the SP scheme is negative charge. This explains the larger flash rates using the SP compared to the TAK scheme. Additionally, it qualitatively appears from Figure 2 that there is much more range in total noninductive charging for the SP simulations than among the TAK simulations, possibly due to greater variability in charge separation sign in the SP scheme. This may explain the weaker correlation coefficients between flash rate and its predictors in the SP simulations than in the TAK simulations. Interestingly, the difference in total negative charge increases among simulation pairs as the total positive charge increases, as indicated by the longer connecting lines with increasing positive charge.

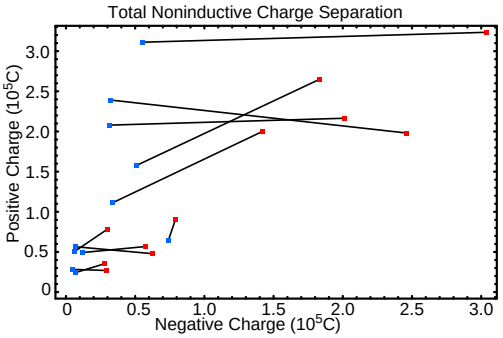

Figure 2: Total temporal and spatial noninductive charge separated, with results from the Saunders-Peck charging scheme in red and from the Takahashi charging scheme in blue.

6. Domain Variations Discussion

To further investigate the impact that non-unicell convection has on reducing the correlation coefficients between flash rate and the other variables specifically for the perturbation quantities, we manually divided the model domain into rectangular subdomains to study these relationships for distinct convective elements of three SP simulations (Table 4). Based on the analysis of the unicell storm cases, one might expect that the correlation coefficients for these cell-tracking subdomains would be higher between the perturbation quantities. Table 4 indicates the correlation coefficients between total flash rate and electric field, graupel volume, and updraft mass flux for both a north and south sector for the first hour or so (S1, N1) of the simulation and then for the second part of the simulation (S2, N2), as well as over the entire domain using the 3-minute history data. It is important to note that model output used for this sector-analysis is based on three-minute sampling over the domain, which may result in smoother time series data than the 1-minute output used for Tables 1–3. Nevertheless, Table 4 still indicates low correlations for the perturbation quantities using 3-minute calculations, just as with 1-minute calculations.

It does appear that individual cells do indeed have better correlations for their perturbation quantities, as evidenced by correlation coefficients in Table 4 being up to 0.4 larger than those Table 3, especially for graupel volume and

Case	EF	GV	UMF
Butler – S1	0.04	0.12	negl.
Butler – N1	0.08	0.29	0.08
Butler – S2	0.03	0.07	0.11
Butler – N2	0.03	0.20	0.12
Butler – All	0.11	negl.	negl.
Franklin – S1	0.01	negl.	0.28
Franklin – N1	0.18	0.04	0.02
Franklin – S2	0.01	0.05	0.05
Franklin – N2	0.04	0.40	0.02
Franklin – All	negl.	0.37	0.19
Hardin – S1	0.11	0.28	0.36
Hardin – N1	0.31	0.19	0.01
Hardin – S2	0.04	0.12	negl.
Hardin – N2	0.01	0.10	0.44
Hardin – All	negl.	0.07	0.18

Table 4: CCs between detrended flash rate and detrended electric field (EF), graupel volume (GV), and updraft mass flux (UMF) for sectorized storms, as well as over the entire domain using 3-minute model output, and with "negl." indicating a neglible value (< 0.01)

updraft mass flux, but still not greater than 0.45. These improvements seem to be dominant for the northern subdomains. Surprisingly, these correlations are also higher for the electric field in some cases. However, the biggest improvement appears to be higher correlations for the updraft mass flux rather than graupel volume, consistent with discussion throughout this entire work. Consideration of fewer stages of various cells' lives in the subdomains compared to the entire domain results in better correlations between the perturbation quantities.

The cell-tracking subdomains were crude rectangles that often included edges of neighboring cells. Thus it is possible that a more careful delineation of a cell could result in more significant correlations. It is also quite possible that the nature of the convection in these cases is simply more variable in time.

7. Conclusions

This study provides an analysis of the relationships between flash rates and several microphysical quantities across an ensemble of simulated storms using two parameterizations of noninductive charge separation. Some of these quantities include electric field, graupel volume, and updraft mass flux, rain mass, crystal mass flux, updraft volume, maximum updraft, and cloud ice mass. Modifications to surface moisture and bulk shear depth and magnitude yielded a wide range of storm intensity and morphology, from weak, unicell storms, to strong squall lines and supercells. Each of the 11 unique cases was run with two different noninductive graupel-ice charge separation schemes, for a total of 22 simulations. Results show that the relationships between total flash rate and rain mass, ice crystal mass flux, and graupel volume are the most significant, while the relationships are weak for electric field and maximum updraft. In cases where convection remained isolated (i.e., one cell in the model domain for most of the 120 minutes), the correlations between detrended total flash rate and graupel volume were also found to be significant. Sectorizing the domain to study individual cells also resulted in higher, but still weak, correlation coefficients, indicating that multiple phases of cells over the domain reduce correlations between the cycles of the variables studied. Additionally, by lagging flash rate time series backwards in time, the correlation coefficients between flash rates and some of the microphysical variables were found to increase slightly. Understanding these relationships can provide the foundation for future work in predicting flash rates across a wide range of storms based on observational information, including radar data.

8. Acknowledgements

Funding for this research was provided under NOAA-Univ. of Oklahoma Cooperative Agreement NA17RJ1227. The authors thank NSSL scientists Dr. Donald MacGorman and Dr. Conrad Ziegler for their helpful support with this paper.

9. Appendix

Figures 3, 4, and 5 show the simulated surface radar reflectivity for the 11 storms.

References

Carey, L. D. and S. A. Rutledge, 1996: A multiparameter radar case study of the microphysical and kinematic evolution of a lightning producing storm. *J. Meteor. Atmos. Phys.*, **59**, 33–64.

Coniglio, M. C., D. J. Stensrud, and L. J. Wicker, 2006: Effects of upper-level shear on the structure and maintenance of strong quasi-linear mesoscale convective systems. *J. Atmos. Sci.*, **63**, 1231–1252.

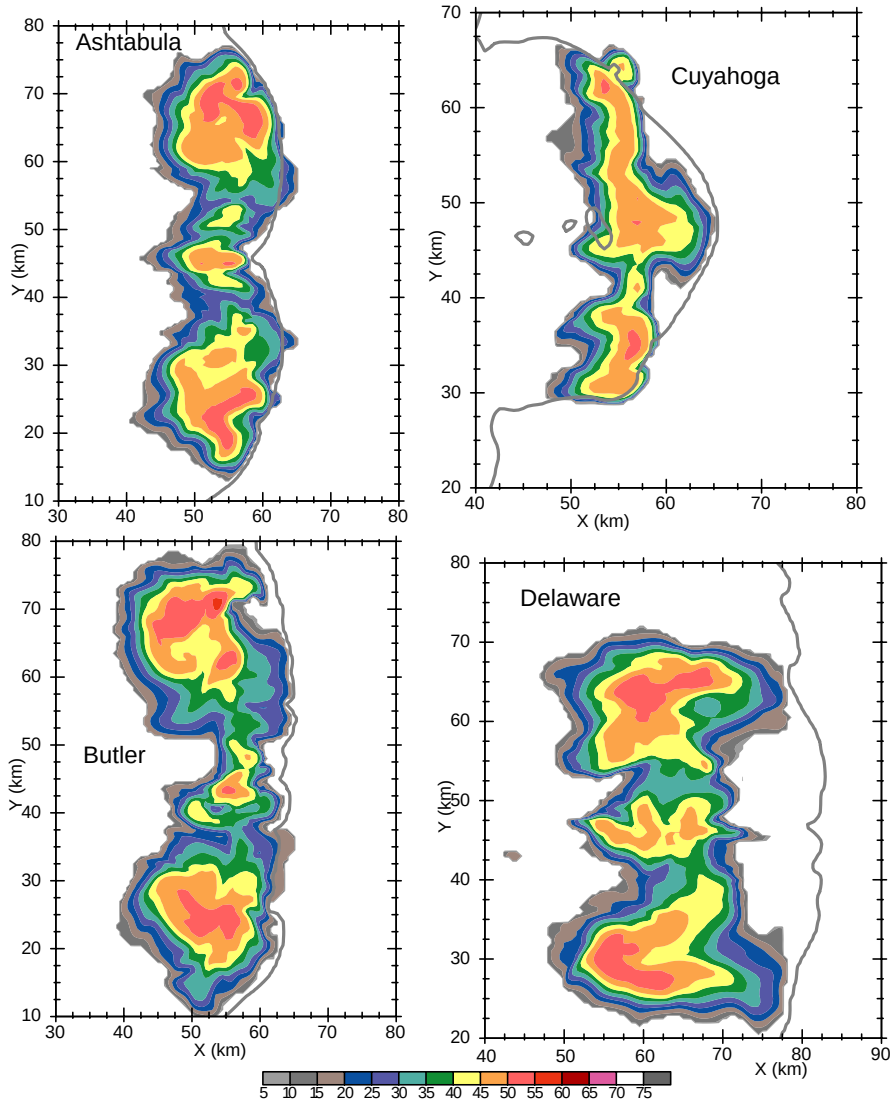

Figure 3: Surface radar reflectivity representations in color and -1 K potential temperature perturbation contour in gray for the first four storms.

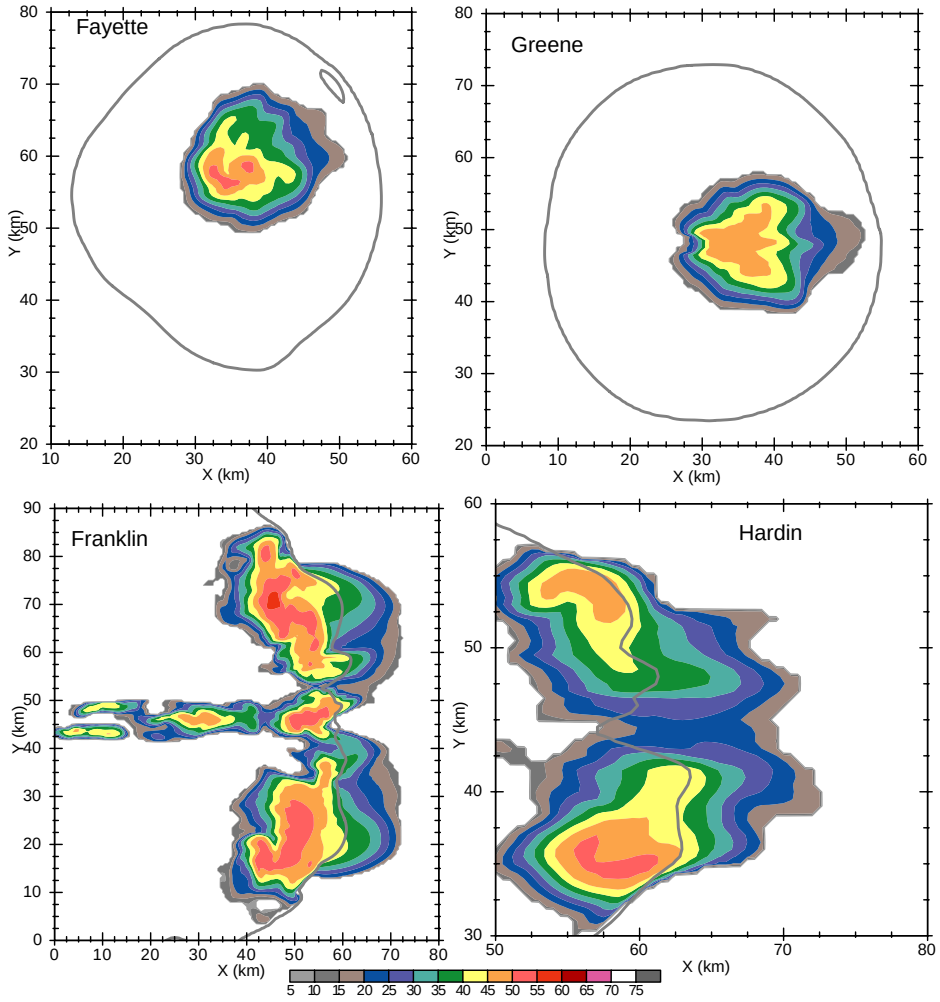

Figure 4: As in Figure 3, but storms 5–8.

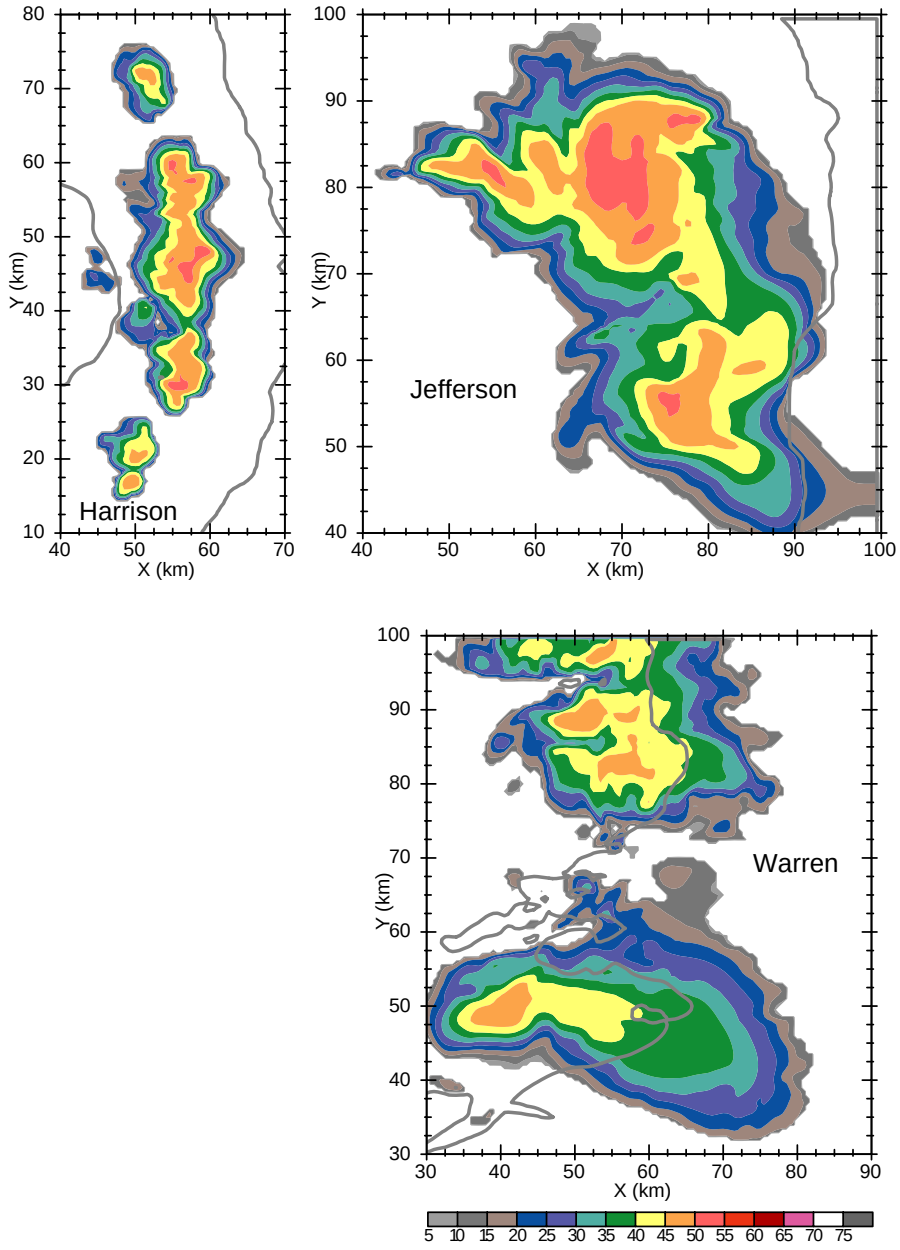

Figure 5: As in Figure 3, but storms 9–11.

Deardorff, J. W., 1980: Stratocumulus-capped mixed layers derived from a three-dimensional model. *Bound.-Layer Meteor.*, **18**, 495–527.

Fierro, A. O., M. S. Gilmore, E. R. Mansell, L. J. Wicker, and J. M. Straka, 2006: Electrification and lightning in an idealized boundary-crossing supercell simulation of 2 June 1995. *Mon. Wea. Rev.*, **134**, 3149–3172.

Gremillion, M. S. and R. E. Orville, 1999: Thunderstorm characteristics of cloud-to-ground lightning at the Kennedy Space Center, Florida: A study of lightning initiation signatures as indicated by the WSR-88D. *Wea. Forecasting*, **14**, 640–649.

Hondl, K. D. and M. D. Eilts, 1994: Doppler radar signatures of developing thunderstorms and their potential to indicate the onset of cloud-to-ground lightning. *Mon. Wea. Rev.*, **122**, 1818–1836.

Kempf, N. M. and E. P. Krider, 2003: Cloud-to-ground lightning and surface rainfall during the great flood of 1993. *Mon. Weather Rev.*, **131**, 1140–1149.

Klemp, J. B. and R. B. Wilhelmson, 1978: The simulations of three-dimensional convective storm dynamics. *J. Atmos. Sci.*, **35**, 1070–1096.

Kuhlman, K. M., C. L. Ziegler, E. R. Mansell, D. R. MacGorman, and J. M. Straka, 2006: Numerically simulated electrification and lightning of the 29 june 2000 STEPS supercell storm. *Mon. Wea. Rev.*, **134**, 2734–2757.

MacGorman, D. R., D. W. Burgess, V. Mazur, W. D. Rust, W. L. Taylor, and B. C. Johnson, 1989: Lightning rates relative to tornadic storm evolution on 22 May 1981. *J. Atmos. Sci.*, **46**, 221–250.

MacGorman, D. R. and W. D. Rust, 1998: *The Electrical Nature of Storms*. Oxford Univ. Press, New York, 422 pp.

Mansell, E. R., D. R. MacGorman, C. L. Ziegler, and J. M. Straka, 2002: Simulated three-dimensional branched lightning in a numerical thunderstorm model. *J. Geophys. Res.*, **107**, doi:10.1029/2000JD000244.

— 2005: Charge structure and lightning sensitivity in a simulated multicell thunderstorm. *J. Geophys. Res.*, **110**, doi:10.1029/2004JD005287.

Mazur, V. and L. H. Ruhnke, 1998: Model of electric charges in thunderstorms and associated lightning. *J. Geophys. Res.*, **103**, 23299–23308.

Petersen, W. A., H. J. Christian, and S. A. Rutledge, 2005: TRMM observations of the global relationship between ice water content and lightning. *Geophys. Res. Lett.*, **32**, doi:10.1029/2005GL023236.

Saunders, C. P. R. and S. L. Peck, 1998: Laboratory studies of the influence of the rime accretion rate on charge transfer during crystal/graupel collisions. *J. Geophys. Res.*, **103**, 13949–13956.

Takahashi, T., 1984: Thunderstorm electrification – a numerical study. *J. Atmos. Sci.*, **41**, 2541–2558.

Weisman, M. L. and J. B. Klemp, 1982: The dependence of numerically simulated convective storms on vertical wind shear and buoyancy. *Mon. Wea. Rev.*, **110**, 504–520.

— 1984: The structure and classification of numerically simulated convective storms in directionally varying wind shears. *Mon. Wea. Rev.*, **112**, 2479–2498.

Wicker, L. J. and W. C. Skamarock, 2002: Time-splitting methods for elastic models using forward time schemes. *Mon. Wea. Rev.*, **130**, 2088–2097.

Wicker, L. J. and R. B. Wilhelmson, 1995: Simulation and analaysis of tornado development and decay within a three-dimensional supercell thunderstorm. *J. Atmos. Sci.*, **52**, 2675–2703.

Wiens, K. C., S. A. Rutledge, and S. A. Tessendorf, 2005: The 29 June 2000 supercell observed during STEPS. Part II: Lightning and charge structure. *J. Atmos. Sci.*, **62**, 4151–4177.

Ziegler, C. L., 1985: Retrieval of thermal and microphysical variables in observed convective storms. Part I: Model development and preliminary testing. *J. Atmos. Sci.*, **42**, 1487–1509.

Zrnić, D. S., N. Balakrishnan, C. L. Ziegler, V. N. Bringi, K. Aydin, and T. Matejka, 1993: Polarimetric signatures in the stratiform region of a mesoscale convective system. *J. Appl. Meteor.*, **32**, 678–693.